Conformational analysis of the natural iron chelator *myo*-inositol 1,2,3-trisphosphate using a pyrene-based fluorescent mimic†

David Mansell,[a] Nicholas Rattray,[a] Laura L. Etchells,[a] Carl H. Schwalbe,[b] Alexander J. Blake,[c] Julia Torres,[d] Carlos Kremer,[d] Elena V. Bichenkova,[a] Christopher J. Barker[e] and Sally Freeman*[a]

Received 19th January 2010, Accepted 7th April 2010
First published as an Advance Article on the web 29th April 2010
DOI: 10.1039/c001078b

myo-Inositol phosphates possessing the 1,2,3-trisphosphate motif share the remarkable ability to completely inhibit iron-catalysed hydroxyl radical formation. The simplest derivative, *myo*-inositol 1,2,3-trisphosphate [Ins(1,2,3)P_3], has been proposed as an intracellular iron chelator involved in iron transport. The binding conformation of Ins(1,2,3)P_3 is considered to be important to complex Fe^{3+} in a 'safe' manner. Here, a pyrene-based fluorescent probe, 4,6-bispyrenoyl-*myo*-inositol 1,2,3,5-tetrakisphosphate [4,6-bispyrenoyl Ins(1,2,3,5)P_4], has been synthesised and used to monitor the conformation of the 1,2,3-trisphosphate motif using excimer fluorescence emission. Ring-flip of the cyclohexane chair to the penta-axial conformation occurs upon association with Fe^{3+}, evident from excimer fluorescence induced by π–π stacking of the pyrene reporter groups, accompanied by excimer formation by excitation at 351 nm. This effect is unique amongst biologically relevant metal cations, except for Ca^{2+} cations exceeding a 1 : 1 molar ratio. In addition, the thermodynamic constants for the interaction of the fluorescent probe with Fe^{3+} have been determined. The complexes formed between Fe^{3+} and 4,6-bispyrenoyl Ins(1,2,3,5)P_4 display similar stability to those formed with Ins(1,2,3)P_3, indicating that the fluorescent probe acts as a good model for the 1,2,3-trisphosphate motif. This is further supported by the antioxidant properties of 4,6-bispyrenoyl Ins(1,2,3,5)P_4, which closely resemble those obtained for Ins(1,2,3)P_3. The data presented confirms that Fe^{3+} binds tightly to the unstable penta-axial conformation of *myo*-inositol phosphates possessing the 1,2,3-trisphosphate motif.

Introduction

myo-Inositol 1,2,3-trisphosphate [Ins(1,2,3)P_3, **1**] is a cellular component in a variety of mammalian cells, present at concentrations of 1–10 μM.[1–5] **1** is of biological interest due to its potent iron chelation and antioxidant properties. The synthesis and iron binding properties of Ins(1,2,3)P_3 were first reported by Spiers and co-workers.[6,7] Ins(1,2,3)P_3 was shown to bind Fe^{3+} with high affinity and completely inhibited Fe^{3+}-catalysed hydroxyl radical formation at ~100 μM, thereby resembling $InsP_6$ and other 1,2,3-trisphosphate containing *myo*-inositol phosphates.[8,9] In view of its remarkable iron chelating and antioxidant properties, Ins(1,2,3)P_3 has been identified as a candidate for a low molecular weight cellular Fe^{3+} "safe" complexing agent.[5,7,10] Indeed, our recent potentiometric studies demonstrated that, unlike the more abundant *myo*-inositol hexa*kis*phosphate ($InsP_6$ ≈ 20 μM[11]), Ins(1,2,3)P_3 fulfils the requirements of a safe, low molecular weight biological Fe^{3+} chelator. Under conditions of excess Mg^{2+} (*e.g.* cytosolic and nuclear regions of mammalian cells), a negligible proportion of $InsP_6$ is bound to Fe^{3+} due to the formation of a neutral pentamagnesium species [$Mg_5(H_2InsP_6)$].[12] In contrast, Fe^{3+} remains fully complexed with Ins(1,2,3)P_3, both under Mg^{2+}-rich conditions and in acidic, Ca^{2+}-rich media such as in lysosomes.[13] Therefore Ins(1,2,3)P_3 possesses the chemical properties expected of an intracellular iron complexing agent. Its capacity to inhibit iron redox cycling and associated production of free radicals is unique to the *myo*-inositol phosphates containing the 1,2,3-trisphosphate motif, and is crucial given the dangers associated with iron-catalysed free radical formation.

The ability of a ligand to inhibit Fe^{3+}-catalysed hydroxyl radical formation is predicted to arise from the occupation of all six coordination sites around iron, thus preventing its participation in the Haber–Weiss redox cycles.[14] The binding conformation of Ins(1,2,3)P_3 with Fe^{3+}, and more specifically the orientation of the phosphate groups is key to bind iron in a 'safe' manner. Ins(1,2,3)P_3 can exist in two chair conformations, orientating the phosphate groups either equatorial–axial–equatorial (**1A**) or axial–equatorial–axial (**1B**) (Scheme 1). The crystal structure of the cyclohexylammonium salt of Ins(1,2,3)P_3, reported by our research group,[15] showed the expected stable penta-equatorial chair conformation. Geometry optimisation calculations for the two chair conformations indicate that the penta-equatorial conformation is 8–30 kcal mol^{-1} energetically more favourable than the penta-axial conformation, depending on the ionic charge of

[a]*School of Pharmacy & Pharmaceutical Sciences, University of Manchester, Oxford Road, Manchester, UK M13 9PT. E-mail: sally.freeman@manchester.ac.uk; Fax: +44 161 275 2396; Tel: +44 161 275 2366*
[b]*School of Life and Health Sciences, Aston University, Birmingham, UK B4 7ET*
[c]*School of Chemistry, The University of Nottingham, University Park, Nottingham, UK NG7 2RD*
[d]*Cátedra de Química Inorgánica, Departamento Estrella Campos, Facultad de Química, Universidad de la República, CC 1157, Montevideo, Uruguay*
[e]*Rolf Luft Research Center for Diabetes and Endocrinology, Karolinska Institutet, SE-171 76, Stockholm, Sweden*
† CCDC reference number 762395. For crystallographic data in CIF or other electronic format see DOI: 10.1039/c001078b

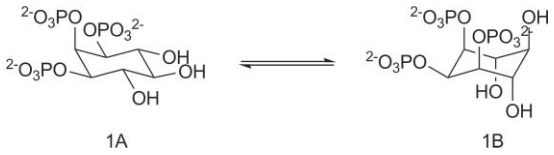

Scheme 1 Penta-equatorial (**1A**) and penta-axial (**1B**) conformations of Ins(1,2,3)P_3.

the molecule.[15,16] A conformational study using ^{1}H-NMR spectroscopy indicated that Ins(1,2,3)P_3 exists in the penta-equatorial conformation across the entire pH range 1.0–13.0.[17] In contrast, it has been proposed by Phillippy and Graf that the Ins(1,2,3)P_3–Fe^{3+} complex adopts the penta-axial conformation, with hexa-coordination of iron by two terminal oxygens from each phosphate group.[18] In this conformation the phosphate groups are orientated axial–equatorial–axial, positioning them closer together than any other combination, which is suggested by the authors as possibly the only orientation that permits hexa-coordination of iron.

It has not been possible to obtain a crystal structure of the Ins(1,2,3)P_3–Fe^{3+} complex. In addition, the application of NMR spectroscopy to study the conformation of the Ins(1,2,3)P_3–Fe^{3+} complex is not possible due to the paramagnetic property of Fe^{3+}. Consequently, alternative approaches are required in order to ascertain structural information on the Ins(1,2,3)P_3–Fe^{3+} complex. To this end, we have designed a fluorescent probe to study the Ins(1,2,3)P_3 motif, using Fe^{3+} complexation as the potential trigger for conformational change (Scheme 2).

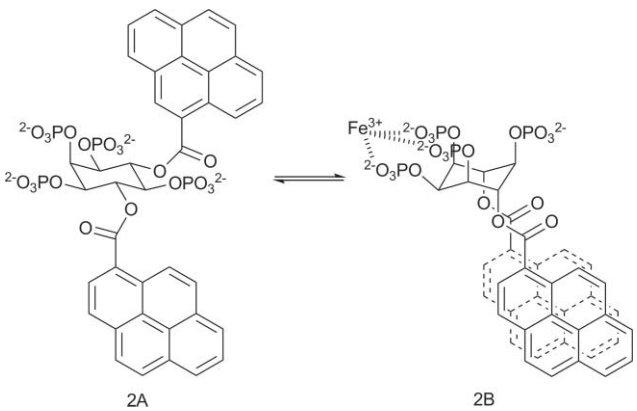

Scheme 2 Conformational ring-flip of 4,6-bispyrenoyl-*myo*-inositol 1,2,3,5-tetrakisphosphate from the penta-equatorial (**2A**) to the penta-axial conformation (**2B**) upon association with Fe^{3+}.

The development of fluorescent iron biosensors is a highly active area of research. Many existing biosensors have been derived from naturally occurring siderophores, either utilising their intrinsic fluorescence or combining siderophore-inspired receptors coupled with fluorescent moieties.[19–24] We have applied this latter concept to our design and developed a probe which combines the 1,2,3-trisphosphate motif and a 4,6-diaxial arrangement of fluorescent pyrene reporter groups. This is based on recent methodology developed in our research group, in which the acid-triggered conformational flip of an orthoformate constrained *myo*-inositol ring was monitored using pyrene excimer fluorescence.[25,26] Similar methodology has also been applied to cyclohexane[27,28] and sugar-based[29,30] metal ion sensors, where chelation with metal cations induces the conformational ring-flip. Initial studies of the fluorescent probe 4,6-bispyrenoyl-*myo*-inositol 1,2,3,5-tetrakisphosphate (**2**) were recently outlined in a communication.[16] This paper describes full details of the synthesis (including the new X-ray crystal structure of a key intermediate) and fluorescence properties of **2**, together with additional studies with relevant metal cations. In addition, the solution complexation behaviour of **2** with Fe^{3+} and its antioxidant properties have been determined.

Results and discussion

A fluorescent probe of *myo*-inositol 1,2,3,5-tetrakisphosphate [Ins(1,2,3,5)P_4] was chosen over the more obvious Ins(1,2,3)P_3 derivative due to its significantly shorter synthesis. This can be justified as Ins(1,2,3,5)P_4 exhibits near identical iron binding properties to Ins(1,2,3)P_3.[7] Furthermore, acid–base studies indicate that the 1,2,3-trisphosphate motif behaves similarly in these inositol phosphates, due to minimal interaction between the 1,2,3-trisphosphate motif and the distant P5 phosphate in Ins(1,2,3,5)P_4.[31] Therefore, a 1,2,3,5-tetrakisphosphate analogue was predicted to represent a good model for the 1,2,3-trisphosphate motif.

Synthesis of 4,6-*O*-bispyrenoyl-*myo*-inositol 1,2,3,5-tetrakisphosphate

The synthesis of the fluorescent probe **2** (Scheme 3) commences with 2-*O*-*tert*-butyldimethylsilyl-*myo*-inositol 1,3,5-orthoformate (**3**), which was reacted with pyrene-1-carboxylic acid, DCC and DMAP to give 2-*O*-(*tert*-butyldimethylsilyl)-4,6-bispyrenoyl-*myo*-inositol 1,3,5-orthoformate (**4**). The synthesis and excimer fluorescence properties of **4** have previously been reported by our group.[25,26] The crystal structure of **4** was reported in our preliminary communication and elegantly demonstrated the π–π stacking of the pyrene rings,[16] and hence rationalises the formation of excimer fluorescence.[25,26] The hydrolysis of the 1,3,5-orthoformate and silyl groups in **4** proceeded smoothly in the presence of one equivalent of *p*-toluenesulfonic acid at 45 °C in THF–methanol (2 : 1).[32] The tetraol product **5** was subsequently treated with dibenzyl *N*,*N*-diisopropylphosphoramidite, followed by oxidation with *m*-chloroperoxybenzoic acid to give **6**. Benzyl deprotection of **6** was achieved by catalytic hydrogenation to generate the free acid **7**, which was converted to the sodium salt (**2**) (Scheme 3).

Crystal structure of 4,6-bispyrenoyl-*myo*-inositol 1,2,3,5-tetrakis(dibenzyl phosphate) 6

Crystals of **6** suitable for structure determination were obtained by slow evaporation of a solution in dichloromethane. As expected, the crystal structure of **6** confirms the penta-equatorial conformation (Fig. 1), in which the pyrene rings extend in different directions with no intramolecular interaction, the angle between their planes being 69.87(4)°. In the crystal structure of **4**,[16] the intramolecular stacking of pyrene rings was facilitated by a series of bond angles that expanded above tetrahedral values: C5–C4–O4, C4–C5–C6 and C5–C6–O6 were 110.7(1), 113.8(1) and 114.5(1)°. In **6** the relaxation allowed by equatorial instead of axial orientation with no intramolecular stacking constraint lets these angles decrease to 107.3(2), 109.0(2) and 107.7(2)°. However, intermolecular interactions are observed between pyrene rings:

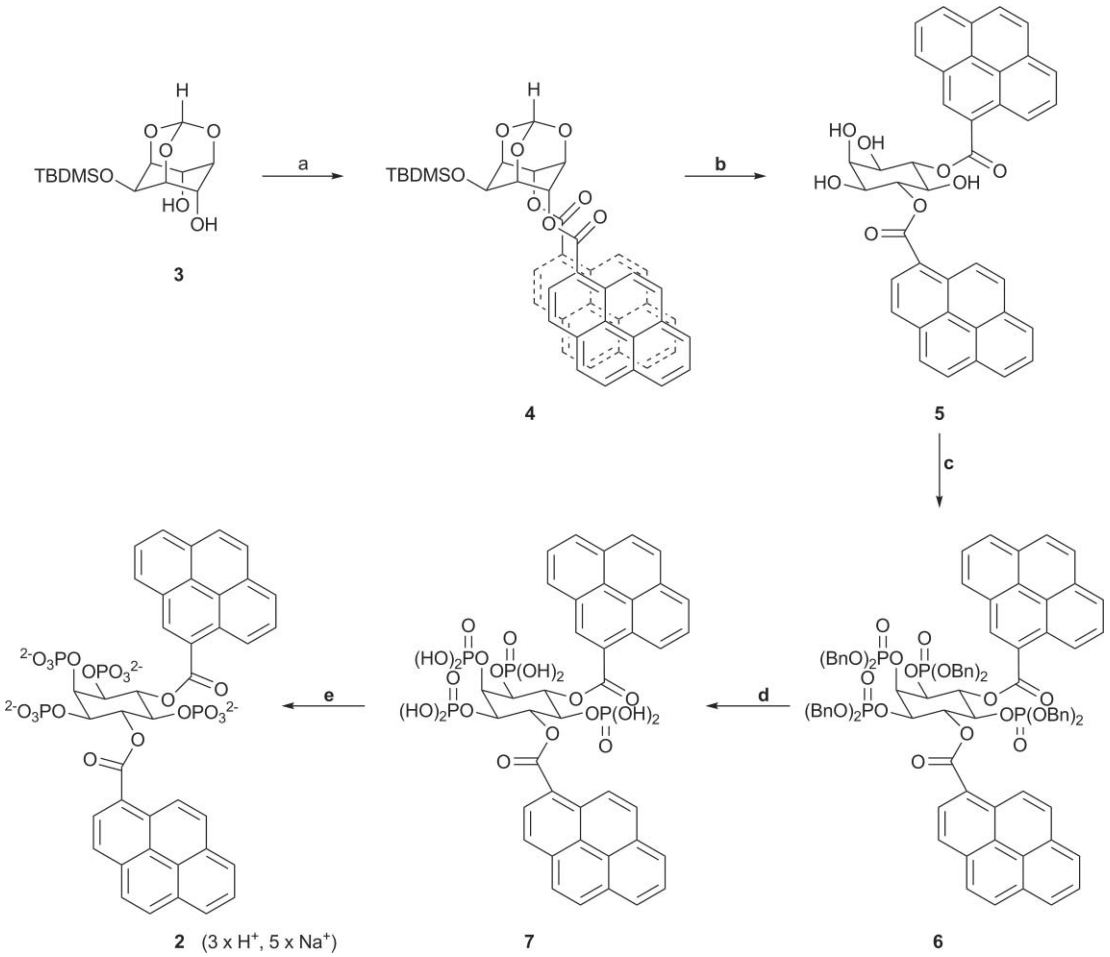

Scheme 3 Synthesis of the fluorescent probe 4,6-bispyrenoyl-*myo*-inositol 1,2,3,5-tetrakisphosphate (**2**): (a) pyrene-1-carboxylic acid, DCC, DMAP, anhydrous DCM; (b) *p*-toluenesulfonic acid, THF–MeOH (2 : 1); (c) i, dibenzyl *N*,*N*-diisopropylphosphoramidite, 0.45 M 1*H*-tetrazole, MeCN; ii, *m*-CPBA, DCM; (d) H_2/Pd–C, ethanol; (e) Dowex 50-X8 resin, mesh 20–50, Na^+ form, elution with water.

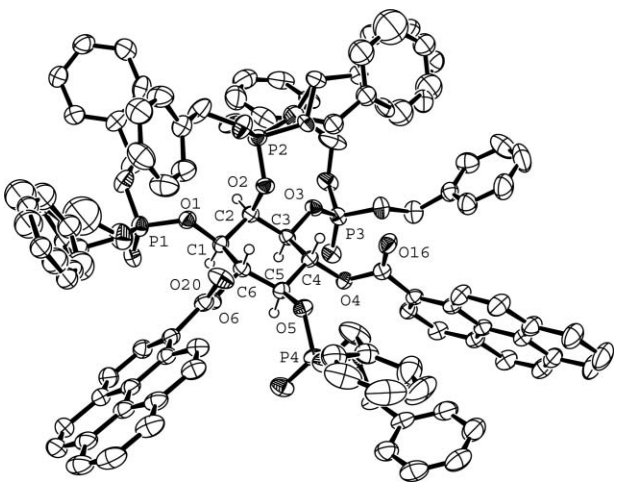

Fig. 1 ORTEP drawing of **6** showing the numbering scheme. Non-inositol hydrogen atoms have been suppressed for clarity, and ellipsoids are drawn at the 50% probability level.

parallel rings of like kind from molecules related by inversion centres are stacked with an offset geometry, as predicted by the Hunter and Sanders[33] model for intermolecular π–π interactions

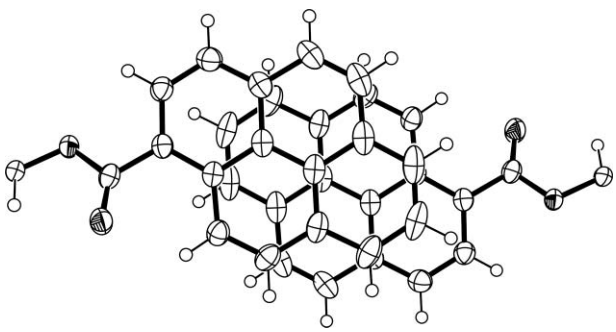

Fig. 2 Stacking of the C80–C96 pyrenoyl system in **6** and its partner related by inversion, viewed normal to the ring plane.

between aromatic molecules (Fig. 2). Packing is sufficiently loose that disorder affects a benzyl group attached to P1 and a benzyloxy group at P2.

A possible concern regarding the use of **2** to model Ins(1,2,3)P_3 as an iron ligand is the conformational effect of its 4,6-pyrenoyl substituents and its extra phosphate group. In **6** there may be further effects from its eight benzyl groups. The three phosphate groups of Ins(1,2,3)P_3, located equatorial–axial–equatorial, were found to cause minimal distortion from an ideal cyclohexane

chair.[15] Alterations in torsion angles within the cyclohexane ring between Ins(1,2,3)P_3 and **6** do not exceed 3.8°. Changes in P···P distances are observed, P1···P2 increasing from 4.263 to 4.717 Å and P2···P3 decreasing from 5.293 to 5.073 Å, widening the overall span between P1 and P3 from 6.836 to 7.326 Å. The inequality of adjacent P···P distances in Ins(1,2,3)P_3, which was studied as the salt with one sodium and four cyclohexylammonium ions, suggests flexibility in response to a strong intramolecular hydrogen bond between positions 1 and 2 and sodium ion coordination at position 3. In **6** the C–O–P=O torsion angles from inositol ring positions 1, 2 and 3 to the terminal O atoms do not exceed ±6.4(2)°. Presumably such an eclipsed conformation is tolerated in order to keep all six benzyl groups free of interference. It is not found at the 5-position, nor in Ins(1,2,3)P_3, and it would not be expected in **2**.

Fluorescence analysis

The emission spectra of **2** in the absence and presence of Fe^{3+} were recorded in methanol at low concentrations (1 μM) to avoid intermolecular interactions. The emission spectrum of **2** in the absence of metal cation (---) shows a blue fluorescence band at 386 nm characteristic of the locally excited state of the pyrene monomer of **2** in the penta-equatorial conformation. However, in the presence of Fe^{3+} (···) a marked disturbance in the fluorescence emission spectrum of **2** is observed, with a substantial decrease in fluorescence of the locally excited state at 386 nm accompanied by the appearance of a new broad emission band at 510 nm (green fluorescence). This is attributed to the excimer emission of two closely located pyrene rings in the penta-axial conformation of **2**. This is indicative of **2** undergoing a ring-flip to the penta-axial conformation upon association with Fe^{3+} (Scheme 2). Owing to the quenching properties of Fe^{3+}, the fluorescence emission spectrum of **2** was also recorded in the presence of Ga^{3+}, a non-quenching analogue of Fe^{3+}.[24,34–36] The trivalent gallium metal cation (d^{10}) possesses similar chemistry to Fe^{3+} (high-spin d^5) and is therefore predicted to behave similarly to Fe^{3+} with respect to its binding to the fluorescent probe. Indeed, the emission spectrum of **2** in the presence of Ga^{3+} (—) (Fig. 3) showed a similar excimer emission peak at 515 nm, but in this case is observed with more than double the intensity of that observed in the presence of Fe^{3+}.

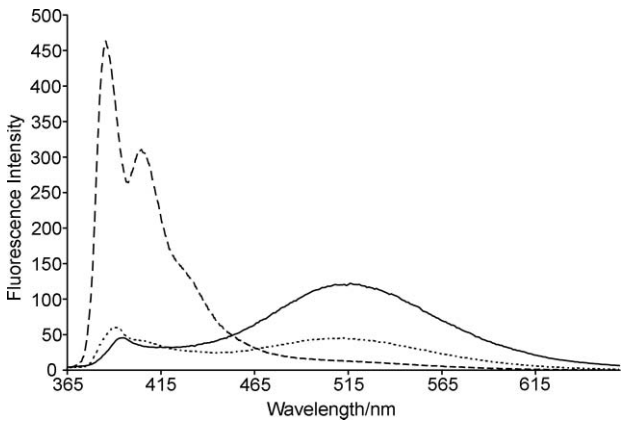

Fig. 3 The fluorescence emission spectra of 4,6-bispyrenoyl-*myo*-inositol 1,2,3,5-tetrakisphosphate (**2**) recorded in the absence (---) and presence of Fe^{3+} (1 equiv.) (···) or Ga^{3+} (1 equiv.) (—). Reprinted from reference 16.

As a control, the fluorescence emission spectra of 4,6-bispyrenoyl *myo*-inositol (**5**) in the absence and presence of Fe^{3+} or Ga^{3+} were recorded to confirm that the observed ring-flip in **2** is driven by the binding of the metal cations to the 1,2,3-trisphosphate motif and not influenced by the effect of the metal cations on the hydrophobic effect of apolar pyrene–pyrene surface interactions, which could potentially stabilise the penta-axial conformation or induce aggregation of multiple molecules of **2**. The fluorescence emission spectrum of **5** in the absence of metal cations closely resembled the corresponding emission spectrum of **2**. In this case, however, addition of either Fe^{3+} or Ga^{3+} did not induce the fluorescence changes observed for **2**, with no excimer peak observed even when the metal was present in excess (25 × molar equivalents). Although we cannot exclude the possibility of some hydrophobic interactions between the two pyrene fluorophore groups in a highly hydrophilic environment, the contribution of such interactions seems insufficient on its own to promote the penta-axial conformation. This supports the conclusion that the propensity of **2** to ring-flip and concomitant excimer formation is triggered by the binding of Fe^{3+} or Ga^{3+} to the 1,2,3-trisphosphate motif in the penta-axial conformation. However, once in the penta-axial conformation (in the presence of Fe^{3+} or Ga^{3+}) the attainment of intramolecular stacking of pyrene rings is likely to confer some extra stability to the complex since repulsion between the apolar pyrene rings and the polar methanol solvent will be minimised.

The effect of other biologically relevant metal cations on the fluorescence characteristics of **2** was also explored (Fig. 4). The fluorescence emission spectra of **2** were recorded in the presence of Na^+, K^+, Mg^{2+}, Ca^{2+} and Fe^{2+} over a range of concentrations with the molar ratio between **2** and metal ions ranging from 1 : 1 to 1 : 10. In the case of Na^+, K^+ and Mg^{2+} cations (Fig. 4A), no change in the peak shape of fluorescence emission was observed across the concentration range studied, which suggested that any interaction of **2** with these cations must be in the penta-equatorial conformation. The presence of one equivalent of Fe^{2+} caused nearly complete quenching of fluorescence at 386 nm (Fig. 4A). In this case, this was not accompanied by the appearance of the excimer emission band at 510 nm, indicating that Fe^{2+} interacts with the penta-equatorial conformation of **2**. For Ca^{2+}, however, excimer emission was observed at concentrations exceeding 1 : 1, indicating binding to the penta-axial conformation (Fig. 4B). However, this behaviour may be attributable to the formation of a *syn*-1,3,5-triaxial trisphosphate chelation cage with Ca^{2+} (Fig. 5). Indeed, the existence of the *syn*-1,3,5-triaxial trisphosphate arrangement, which form chelation 'cages' with counter-ions, is considered to be a major factor in the ring inversion process of inositol phosphates.[37]

Thermodynamic properties of 4,6-bispyrenoyl Ins(1,2,3,5)P_4 (2)

We have recently described the metal complexation behaviour of Ins(1,2,3)P_3 using high-resolution potentiometry to determine the thermodynamic constants in the presence of multivalent cations.[13] Here, the protonation constants of **2** and its complexation behaviour with Fe(III) cations have been determined under identical conditions (*i.e.* the non-interacting medium 0.15 M NMe_4Cl and 37.0 °C). This was aimed at further testing whether the 1,2,3,5-tetrakisphophate fluorescent probe represents a viable model for

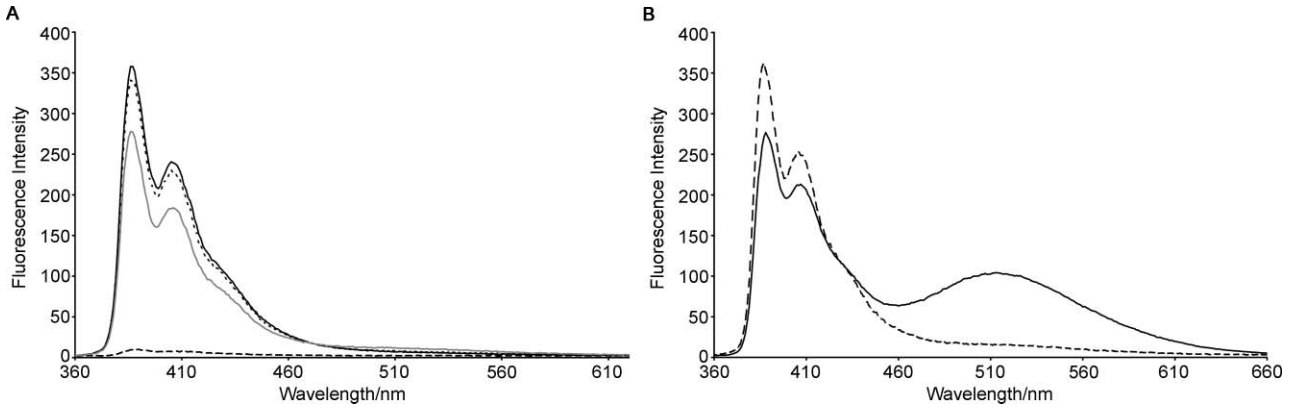

Fig. 4 (A) Emission spectra of 4,6-bispyrenoyl-*myo*-inositol 1,2,3,5-tetrakisphosphate (**2**) in the presence of Na^+ (—), K^+ (···), Fe^{2+} (---) and Mg^{2+} (—). Data are shown for spectra recorded at a concentration of 1 μM in methanol at 20 °C with a 1 : 1 molar ratio of metal cation. (B) Emission spectra of 4,6-bispyrenoyl-*myo*-inositol 1,2,3,5-tetrakisphosphate (**2**) in the presence Ca^{2+}. Data shown are for spectra recorded at a concentration of 1 μM in methanol at 20 °C with 1 : 1 (---) and 1 : 2 (—) (**2** : Ca^{2+}) molar ratio of metal cation. Excitation and emission slit width was 3 nm (**2** : M^{n+}; 1 : 1) and 5 nm (**2** : Ca^{2+}; 1 : 2).

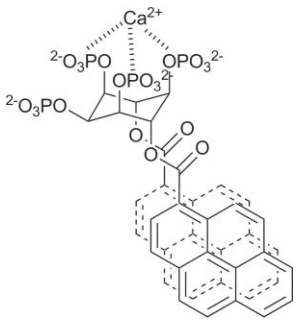

Fig. 5 Ca^{2+} cations may form a chelation cage with the *syn*-1,3,5-triaxial trisphosphate arrangement, inducing a conformational ring flip.

the 1,2,3-trisphosphate motif and assessing its potential as a fluorescent iron probe.

Protonation equilibria of 4,6-bispyrenoyl Ins(1,2,3,5)P_4 (2)

The values for the protonation equilibrium constants are required in order to study the complexation reactions with Fe(III). The fully protonated form of 4,6-bispyrenoyl Ins(1,2,3,5)P_4, H_8L, can be considered as an acid with eight removable protons. Only the first six of these protonation reactions were determined here, the last two not being amenable to the methods used, due to the low solubility of the system in strong acidic media (Table 1).

The log *K* values determined followed the expected order and are consistent with previously reported values for the chemically related Ins(1,2,3,5)P_4.[31] For Ins(1,2,3,5)P_4 only four protonation constants were measured, also by potentiometric measurements but performed in 0.2 M KCl at 37.0 °C.[31] A species distribution diagram for 4,6-bispyrenoyl Ins(1,2,3,5)P_4 *vs.* pH is shown in Fig. 6. For neutral pH values, the predominant species are H_3L^{5-} and H_4L^{4-}.

Interaction between 4,6-bispyrenoyl Ins(1,2,3,5)P_4 (2) and Fe(III)

The complexation of 4,6-bispyrenoyl Ins(1,2,3,5)P_4 with Fe(III) in 0.15 M NMe_4Cl, at 37.0 °C was studied and the equilibrium constants for the complexes formed are shown in Table 1. The complexes formed between Fe(III) and 4,6-bispyrenoyl Ins(1,2,3,5)P_4 showed high stability, which is reflected in the species distribution diagram obtained under similar conditions to those used for some of the potentiometric titrations (0.3 mM ligand, 0.2 mM Fe(III)) (Fig. 7). Hydrolysis reactions are important competing processes for complexation. Under acidic conditions at pH values below 5, the ligand is protonated and the metal ion forms hydroxylated species. In contrast, in the pH range 5.0–9.0 4,6-bispyrenoyl

Table 1 Equilibrium constant logarithms of 4,6-bispyrenoyl Ins(1,2,3,5)P_4 (**2**) alone and in the presence of Fe(III). Data were measured in 0.15 M Me_4NCl at 37.0 °C

Equilibrium[a]	log *K*	Equilibrium[b]	log *K*
$L^{8-} + H^+ \rightarrow HL^{7-}$	9.47(6)	$Fe^{3+} + L^{8-} \rightarrow [FeL]^{5-}$	23.83(5)
$L^{8-} + 2\ H^+ \rightarrow H_2L^{6-}$	18.61(5)	$Fe^{3+} + HL^{7-} \rightarrow [Fe(HL)]^{4-}$	21.13(6)
$L^{8-} + 3\ H^+ \rightarrow H_3L^{5-}$	27.10(6)	$Fe^{3+} + L^{8-} + H_2O \rightarrow [FeL(OH)]^{6-} + H^+$	15.03(3)
$L^{8-} + 4\ H^+ \rightarrow H_4L^{4-}$	34.00(9)	$Fe^{3+} + L^{8-} + 2\ H_2O \rightarrow [FeL(OH)_2]^{7-} + 2\ H^+$	4.88(7)
$L^{8-} + 5\ H^+ \rightarrow H_5L^{3-}$	40.28(8)		
$L^{8-} + 6\ H^+ \rightarrow H_6L^{2-}$	44.5(1)		

[a] $\sigma = 0.8$. [b] $\sigma = 1.3$.

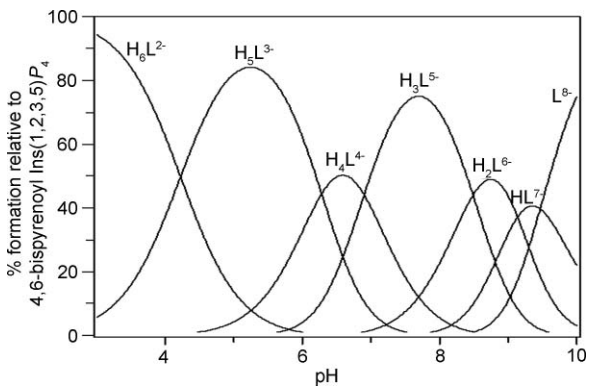

Fig. 6 Species distribution diagram for 4,6-bispyrenoyl Ins(1,2,3,5)P_4 (**2**, 1 mM) in 0.15 M Me_4NCl, and 37.0 °C.

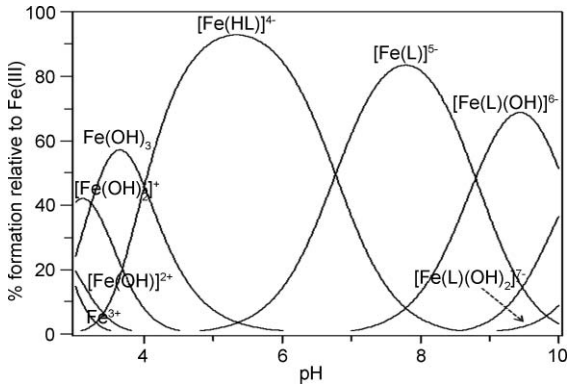

Fig. 7 Species distribution diagram for 4,6-bispyrenoyl Ins(1,2,3,5)P_4 (**2**, 0.3 mM) interaction with Fe(III) (0.2 mM) in 0.15 M Me_4NCl, and 37.0 °C. Fe(III) represents the total iron amount available for complexation.

Ins(1,2,3,5)P_4 iron complexes predominate in the form $[Fe(HL)]^{4-}$ and $[Fe(L)]^{5-}$.

A direct comparison of the stability constants of Ins(1,2,3)P_3 and 4,6-bispyrenoyl Ins(1,2,3,5)P_4 showed that both ligands bear a very high affinity towards Fe^{3+}: 4,6-bispyrenoyl Ins(1,2,3,5)P_4 forms even more stable complexes with Fe^{3+} than Ins(1,2,3)P_3. For example, log K_{110} is 23.83 for 4,6-bispyrenoyl Ins(1,2,3,5)P_4 and 19.04 for Ins(1,2,3)P_3. This difference can be attributed to the presence of an additional phosphate group in 4,6-bispyrenoyl Ins(1,2,3,5)P_4, which enhances the negative charge of the ligand, and also the spatial disposition with the four phosphate groups being on the same side of the ligand in the penta-axial conformation. Alternatively, this additional stability in the 4,6-bispyrenoyl Ins(1,2,3,5)P_4–Fe^{3+} complex may be a reflection of the hydrophobic interactions between the two pyrene groups, stabilising the penta-axial conformation in the probe.

The thermodynamic data allowed the investigation of the ligand 4,6-bispyrenoyl Ins(1,2,3,5)P_4 as a possible Fe^{3+} fluorescent probe.[16] If a thousand-fold excess of ligand was added to a mean overall cellular iron concentration (1 μM), the metal ion was fully complexed in the pH range 5.0–9.0 (Fig. 8). The negative logarithm of the Fe(III) concentration left free at pH 7.4, *i.e.* pFe, is 18.8 ([IP3] = 10 μM, [Fe(III), total] = 10 μM). Furthermore, if the solubility value was added for iron hydroxide,[38] the same result was observed (plot not shown). No iron hydroxide is formed under these conditions, even for iron concentrations up to 30 μM.

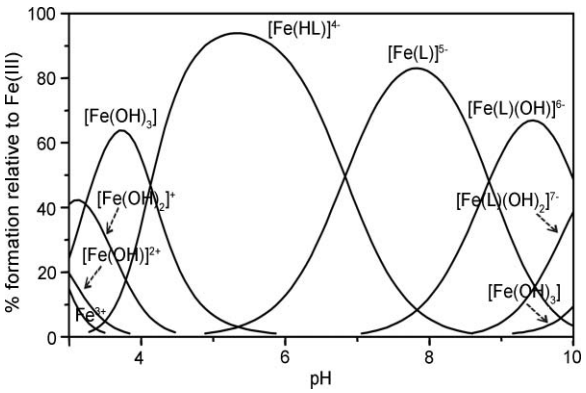

Fig. 8 4,6-Bispyrenoyl Ins(1,2,3,5)P_4 (1 mM) probe interaction with Fe(III) (1 μM) in 0.15 M Me_4NCl, and 37.0 °C. Fe(III) represents the total iron amount available for complexation.

Antioxidant function of 4,6-bispyrenoyl Ins(1,2,3,5)P_4 (2)

Further insight into the iron complex formed with **2** was obtained by evaluating the antioxidant properties of the fluorescent probe. The effect of 4,6-bispyrenoyl Ins(1,2,3,5)P_4 (**2**) on iron-catalysed hydroxyl radical formation was studied using an assay for the Haber–Weiss reaction. The assay conditions were based on literature described by Hawkins and co-workers[9] and Graf and co-workers,[8,14] utilising a hypoxanthine/xanthine oxidase system for HO• generation. The HO• reacts with DMSO (present in the assay) to give formaldehyde which is measured by a colorimetric assay. Compound **2** was able to completely inhibit Fe^{3+}-catalysed hydroxyl radical formation at ~100 μM (Fig. 9), thereby resembling Ins(1,2,3)P_3 and Ins(1,2,3,5)P_4. Since the 1,2,3-trisphosphate motif is necessary and sufficient to induce complete inhibition of Fe^{3+}-catalysed HO• formation, this indicates that Fe^{3+} must bind to 4,6-bispyrenoyl Ins(1,2,3,5)P_4 in a similar manner to Ins(1,2,3)P_3. Therefore, in support of the thermodynamic data described above, which indicate that 4,6-bispyrenoyl Ins(1,2,3,5)P_4 displays a similar affinity for Fe^{3+} to that of Ins(1,2,3)P_3, we can conclude that the fluorescent probe is an appropriate model for the 1,2,3-trisphosphate motif.

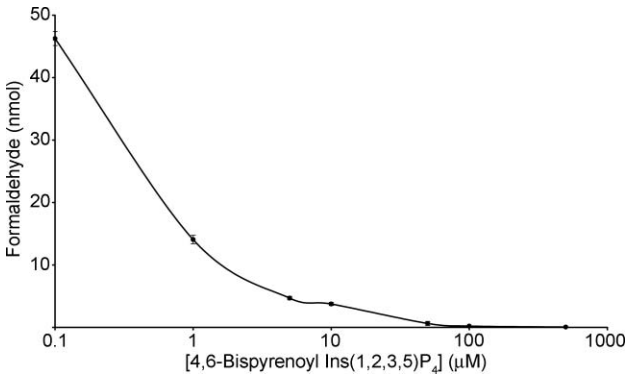

Fig. 9 Effect of 4,6-bispyrenoyl Ins(1,2,3,5)P_4 (**2**) on HO• generation. The result shown is typical of three independent experiments.

Conclusion

We have developed a pyrene-based fluorescent probe (**2**) possessing a 4,6-bispyrenoyl arrangement that can detect the conformational ring-flip of the *myo*-inositol ring upon association of the 1,2,3-trisphosphate motif with Fe^{3+}. In the absence of Fe^{3+}, the pyrenoyl substituents are positioned in a 4,6-diequatorial conformation, with blue fluorescence observed at 386 nm attributed to the locally excited state of the pyrene monomer. Synchronous with Fe^{3+} chelation, the diequatorial pyrenoyl substituents are rearranged into the 4,6-diaxial conformation, promoting excimer fluorescence and the appearance of a new broad emission band at 510 nm (green fluorescence). This effect was more pronounced when the fluorescence emission spectrum of **2** was recorded in the presence of Ga^{3+} (d^{10}), which is a non-quenching analogue of Fe^{3+} (high-spin d^5).[24,34–36]

The thermodynamic stability constants of complexes formed between **2** and Fe^{3+} were determined under the same conditions employed for the study with Ins(1,2,3)P_3.[13] A comparison of the stability constants of Ins(1,2,3)P_3 and 4,6-bispyrenoyl Ins(1,2,3,5)P_4 (**2**) showed that both ligands have a very high affinity towards Fe^{3+}. In addition, complete inhibition of Fe^{3+}-catalysed HO$^{\bullet}$ formation was achieved by **2** at ~100 μM, thereby resembling Ins(1,2,3)P_3 and Ins(1,2,3,5)P_4. These results support the prediction that **2** is a good model for the 1,2,3-trisphosphate motif.

This study provides evidence that Fe^{3+} binding to *myo*-inositol phosphates possessing the 1,2,3-trisphosphate motif is achieved by the *myo*-inositol ring adopting the penta-axial conformation.

Experimental

Material and methods

Reagents and solvents were purchased from Aldrich Chemical Co. (Dorset, UK), VWR International (Leicestershire, UK) and Fisher Scientific (Leicestershire, UK). Deuterated solvents and tetramethylsilane (TMS) were obtained from Cambridge Isotope Laboratories Inc. (Andover, USA). Thin layer chromatography was performed on pre-coated silica gel 60 F_{254} aluminium backed plates (layer thickness 0.2 mm) (Merck). Spots were visualised by ultraviolet radiation at 254 nm and 325 nm using a UV GL-58 mineral light lamp or by staining with $KMnO_4$ solution. Melting points (Mp) were determined in open glass capillary tubes on a GallenKamp MPD.350.BM2.5 apparatus microscope (UK) and are uncorrected. Infra-red spectra were recorded on neat samples using a JASCO FT/IR 4100 instrument. NMR spectra were recorded using a Bruker Avance-300 spectrometer operating at 300 MHz (^{1}H-NMR), 75 MHz (^{13}C-NMR) or 121 MHz (^{31}P-NMR) at 293 K, unless otherwise stated. The spectrometer was running TOPSPIN NMR system software (Version 2.0). Chemical shifts (δ) are reported in parts per million (ppm). ^{1}H-NMR and ^{13}C-NMR spectra were referenced to Me_4Si (0.00 ppm), unless otherwise stated. ^{31}P-NMR spectra were referenced to 85% phosphoric acid. ^{1}H-NMR spectra were assigned with the aid of COSY experiments and ^{13}C-NMR spectra were assigned with the aid of Distortionless Enhanced through Polarisation Transfer (DEPT) experiments. Mass spectra (MS) were recorded at the School of Chemistry, University of Manchester (UK), using Micromass PLATFORM II instrument. Elemental analyses were recorded in the School of Chemistry, University of Manchester (UK), using an EA 1108 Elemental Analyser (Carlo Erba Instrument). Na was quantified by atomic spectroscopy. Thermal analysis was performed on a Shimadzu DTA-50, TGA-50 instrument with a TA 50I interface, using a platinum cell and nitrogen atmosphere. Experimental conditions were 1 °C min^{-1} temperature ramp rate and 50 mL min^{-1} nitrogen flow rate.

Synthesis

4,6-Bispyrenoyl-*myo*-inositol (5). A solution of 2-*O*-(*tert*-butyldimethylsilyl)-4,6-*O*-bispyrenoyl-*myo*-inositol 1,3,5-orthoformate (4)[26] (0.84 g, 1.12 mmol) and *p*-toluenesulfonic acid monohydrate (0.25 g, 1.31 mmol) in THF (30 mL) and methanol (15 mL) was heated at 45 °C for 12 h. The reaction mixture was allowed to cool to room temperature and the product precipitated from chloroform (200 mL). The solid was filtered and washed with chloroform (3 × 30 mL) to give 4,6-bispyrenoyl-*myo*-inositol (**5**) as a yellow solid (0.51 g, 73%). Mp 226–228 °C. δ_H(d_6-DMSO): 3.87 (2H, ddd~t, H-1/3, $^3J_{1/3\text{-}2} \approx {}^3J_{1/3\text{-}4/6} \approx J_{H\text{-}OH}$ 8.3 Hz), 3.93–4.05 (2H, m, H-2 + H-5), 5.11 (2H, d, 2 × OH, $J_{OH\text{–}H}$ 6.3 Hz, exchangeable with D_2O), 5.37 (1H, br s, OH), 5.66 (2H, t, H-4/6, $^3J_{4/6\text{-}1/3} \approx {}^3J_{4/6\text{-}5}$ 9.8 Hz), 5.75 (1H, d, OH, $J_{H\text{-}OH}$ 6.0 Hz), 8.17 (2H, t, Pyr-H, J 7.6 Hz), 8.23-8.48 (m, 12H, Pyr-H), 8.67 (2H, d, Pyr H-15, J 8.67 Hz), 9.11 (2H, d, Pyr H-7, J 9.1 Hz). Additional data for compound **5** have been reported.[26]

4,6-Bispyrenoyl-*myo*-inositol 1,2,3,5-tetrakis(dibenzyl phosphate) (6). Dibenzyl *N*,*N*-diisopropylphosphoramidite (0.84 mL, 2.51 mmol) was added to a solution of 4,6-bispyrenoyl-*myo*-inositol (**5**) (0.20 g, 0.31 mmol) and 1*H*-tetrazole (11.2 mL ~0.45 M in acetonitrile, 5.03 mmol). The mixture was stirred at room temperature under argon for 4 h. The reaction mixture was cooled to −40 °C and a solution of 3-chloroperoxybenzoic acid (1.30 g, ~7.54 mmol) in anhydrous DCM (40 mL) was added dropwise. The reaction mixture was stirred at 0 °C for 2 h. The reaction mixture was diluted with DCM (100 mL), washed with 10% w/v Na_2SO_3 (aq) (2 × 40 mL), sat. $NaHCO_3$ (aq) (2 × 40 mL) and brine (1 × 40 mL), and dried over $MgSO_4$. The solvent was removed under reduced pressure and the residue purified by flash column chromatography (ethyl acetate–DCM, 1 : 1 → 2 : 1). 4,6-Bispyrenoyl-*myo*-inositol 1,2,3,5-tetrakis(dibenzyl phosphate) (**6**) was isolated as an orange solid (0.33 g, 63%). Mp 188–190 °C. Anal. Calcd. for $C_{96}H_{80}O_{20}P_4$: C 68.73; H 4.82%. Found: C 68.17; H 4.82%. IR absorptions: ν_{max}/cm^{-1} 1722 (m, C=O), 1280 (m), 1250 (m), 1227 (m, P=O), 1000 (s, P–O-Bn). δ_H($CDCl_3$): 4.23 (2H, dd, P–O–C*H*$_2$Ph, J_{PH} 11.8 Hz, J_{HH} 7.8 Hz), 4.32 (2H, dd, P–O–C*H*$_2$Ph, J_{PH} 11.7 Hz, J_{HH} 8.4 Hz), 4.51 (2H, dd, P–O–C*H*$_2$Ph, J_{PH} 8.9 Hz, J_{PH} 7.2 Hz), 4.55 (2H, dd, P–O–C*H*$_2$Ph, J_{PH} 8.9 Hz, J_{HH} 7.1 Hz), 4.97–5.13 (6H, m, 2 × P–O–C*H*$_2$Ph + H-1/3), 5.29 (1H, q, H-5, $^3J_{5\text{-}4/6} \approx J_{PH}$ 9.6 Hz), 5.36 (4H, d, 2 × P–O–C*H*$_2$Ph, J_{PH} 5.9 Hz), 5.66 (1H, tt, H-2, J_{PH} 9.1 Hz, $^3J_{2\text{-}1/3}$ 2.0 Hz), 6.32 (4H, d, Ph-*ortho*, J 7.4 Hz), 6.40 (4H, d, Ph-*ortho*, J 7.4 Hz), 6.42–6.65 (14H, m, 12 × Ph + H-4/6), 7.10–7.23 (10H, m, Ph), 7.29–7.38 (6H, m, Ph), 7.43–7.54 (4H, m, Ph), 7.99–8.30 (14H, m, pyr), 8.98 (2H, d, pyr-H, J 8.2 Hz), 9.31 (2H, d, pyr-H, J 9.4 Hz). δ_C($CDCl_3$): 69.0 (d, J_{PC} 5.6 Hz, 2 × Ph*C*H$_2$OP), 69.4 (d, J_{PC} 5.7 Hz, 2 × Ph*C*H$_2$OP), 69.7 (d, J_{PC} 5.6 Hz, 2 × Ph*C*H$_2$OP), 70.0 (d, J_{PC} 6.2 Hz, 2 × Ph*C*H$_2$OP), 70.2 (br s, 2 × inositol CH), 73.9 (br s, 2 × inositol CH), 76.0 (br s, inositol CH), 77.2 (s, inositol CH), 121.4 (s, quat. pyr), 124.1 (s, quat. pyr), 124.3 (s, aromatic CH), 124.7 (s, quat. pyr), 124.8, 126.2, 126.3, 126.7, 126.9, 127.2, 127.4, 127.6, 128.0, 128.2, 128.3, 128.4, 128.5, 129.4, 129.7, 129.8 (all s, aromatic CH), 130.3 (s, quat. pyr), 130.9 (s, quat. pyr), 131.9 (s, quat. pyr), 134.4 (d, J_{PC} 7.1 Hz, quat. *Ph*CH$_2$OP), 134.5 (d, J_{PC} 8.1 Hz, quat. *Ph*CH$_2$OP), 134.8 (s, quat. pyr), 135.5 (d, J_{PC} 8.1 Hz, quat. *Ph*CH$_2$OP), 135.8 (d, J_{PC} 8.9 Hz, quat. *Ph*CH$_2$OP), 166.0 (C=O). δ_P($CDCl_3$): −0.95 (s, *P*$\bar{1}$,3), −1.07 (s, P-2), −2.62 (s, P-5). δ_P($CDCl_3$, ^{1}H-coupled)): −0.95 (sextet, J_{PH} 7.6 Hz), −1.08 (sextet, J_{PH} 7.5 Hz), −2.60 (m). MS (electrospray) *m*/*z* [M+NH_4]$^+$ 1695.

Pentasodium 4,6-bispyrenoyl-*myo*-inositol 1,2,3,5-tetrakisphosphate (2). A mixture of 4,6-bispyrenoyl-*myo*-inositol 1,2,3,5-tetrakis(dibenzyl phosphate) (**6**) (0.10 g, 0.06 mmol) and Pd–C

(10%, 0.02 g) was stirred in ethanol under a hydrogen atmosphere for 24 h at room temperature. The catalyst was removed by filtration through a pad of Celite and the solvent removed under reduced pressure. The residue was dissolved in water (2 mL) and the solution applied to a cation-exchange resin (Dowex 50-X8, mesh 20–50, 10 mL, Na^+ form) and eluted with water (50 mL). The eluent was concentrated to ~3 mL and lyophilised to give the pentasodium salt of 4,6-bispyrenoyl-*myo*-inositol 1,2,3,5-tetrakisphosphate (**2**) as a green solid (0.05 g, 70%). Mp > 300 °C. Anal. calcd. for $C_{40}H_{27}O_{20}P_4Na_5{\cdot}7H_2O$: C 40.28; H 3.47; P 10.39; Na 9.64%. Found: C 40.43; H 2.84; P 10.05; Na 9.60%. Thermal analysis agreed with the proposed formula: Found 10.6% weight loss, which was identical to the expected value, corresponding to the elimination of seven molecules of water. It is recognised that the % hydrogen is beyond acceptable error limits; however, data obtained from potentiometric titrations also supported the proposed molecular formula. IR absorptions: ν_{max}/cm^{-1} 3348 (br, OH), 1703 (C=O), 1257. δ_H(333.2 K, D_2O, referenced to DMSO at 2.71 ppm): 4.34 (2H, ddd~ br t, H-1/3, $J_{PH} \approx {}^3J_{1/3\text{-}4/6}$ 7.0 Hz, coupling to H-2 not observed), 4.56 (1H, dt, H-5, J_{PH} 9.9 Hz, ${}^3J_{5\text{-}4/6}$ 6.9 Hz), 4.86 (1H, dt, H-2, J_{PH} 10.1 Hz, ${}^3J_{2\text{-}1/3}$ 2.7 Hz), 5.57 (2H, t, H-4/6, ${}^3J_{4/6\text{-}1/3} \approx {}^3J_{4/6\text{-}5}$ 7.0 Hz), 7.10–7.79 (14H, m, Pyr-H), 8.07 (2H, br s, Pyr-H), 8.27 (2H, br s, Pyr-H). δ_C(333.2 K, D_2O, referenced to DMSO at 39.39 ppm, poor resolution): 72.6 -73.0 (m, 3 × inositol CH), 73.3–73.6 (m, 3 × inositol CH), 123.1 (Cq, pyr), 123.7 (Cq, pyr), 124.4, 126.4, 126.7, 127.0, 128.8, 129.7, 129.9 (all CH, Pyr), 130.3 (Cq, Pyr), 130.6 (Cq, Pyr) 134.2 (Cq, Pyr), 168.9 (C=O). $\delta_P(D_2O)$: 1.79 (1P), -0.09 (2P), -1.08 (1P). MS (electrospray) m/z [$(C_{40}H_{28}Na_3O_{20}P_4)^-$; free acid + $3Na^+ - 4H^+$] 1021, [$(C_{40}H_{29}Na_2O_{20}P_4)^-$; free acid + $2Na^+ - 3H^+$] 999.

Crystal structure determination

Colourless columnar crystals of 6 were obtained by slow evaporation of DCM solvent. A single crystal (0.09 × 0.16 × 0.28 mm) was used for X-ray structure determination, with diffraction data being collected at low temperature (150 K) on a Bruker SMART APEX CCD area detector, with monochromated graphite Mo-Kα radiation, $\lambda = 0.71073$ Å.

Crystal data. $C_{96}H_{80}O_{20}P_4$, $Mr = 1677.48$ gmol^{-1}, triclinic, space group $P\bar{1}$, $a = 15.160(2)$, $b = 15.211(2)$, $c = 19.507(2)$ Å, $\alpha = 69.540(2)$, $\beta = 83.666(2)$, $\gamma = 77.071(2)°$, $V = 4105(1)$ Å^3, $Z = 2$, $T = 150$ K, $D = 1.357$ (calc.), $\mu = 0.164$ mm^{-1}. 37061 reflections measured, 18574 unique ($R_{int} = 0.031$). The structure was solved by direct methods with SHELXS97[39] and refined by full-matrix least-squares with SHELXL97[39] to $R = 0.0595$ for 11805 reflections with $F_o > 4\sigma(F_o)$, $wR(F^2) = 0.1540$ for all 18574 reflections. Non-hydrogen atoms were refined with anisotropic displacement parameters except for the minor components of disorder, which were kept isotropic. All hydrogen atoms were assumed to ride on their attached atoms.

Fluorescence measurements

Fluorescence emission and excitation spectra were recorded in quartz thermostatted cuvettes of 1 cm path length using a Shimadzu RF-5301PC spectrofluorophotometer. The light source was supplied *via* a 150 W Xenon bulb. Data were processed using Shimadzu RF-5301PC software. Fluorescence spectra of **2** were recorded at a concentration of 1 μM in methanol at 20 °C with an excitation wavelength of 351 nm (determined by UV-spectroscopy). Excitation and emission slit widths were 3 nm (to detect monomer emission) and 5 nm (to detect excimer emission). In the absence of metal: a final volume of 1 mL contained 1 μM of **2** (added from 100 μM stock solution) in methanol. In the presence of metal: a final volume of 1 mL contained 1 μM of **2** (added from 100 μM stock solution) and varying concentrations of metal (added from a 100 μM stock solution) in methanol.

Potentiometric measurements

$Fe(ClO_4)_3{\cdot}xH_2O$ was used as the metal source. Solutions of the metal were standardised according to standard techniques. The standard HCl solution was prepared from Merck standard ampoules, and standardised with $Na_2B_4O_7{\cdot}12H_2O$. The standard solution of $Me_4N(OH)$ was prepared by dissolving $Me_4N(OH){\cdot}5H_2O$ (Fluka), and standardised with potassium biphthalate. All solutions were freed of carbon dioxide by bubbling through with Argon. The ionic strength was adjusted to 0.15 M by adding Me_4NCl. The protonation constants of 4,6-bispyrenoyl Ins(1,2,3,5)P_4 (**2**) were determined at 37.0 °C, 0.15 M ionic strength in the non-interacting electrolyte Me_4NCl. Four potentiometric titrations, comprising 100–150 experimental points each, were carried out in the 4,6-bispyrenoyl Ins(1,2,3,5)P_4 concentration interval 0.2–0.6 mM, covering pH values between 2.5 and 10.0. Below pH 2.5–3.0 (depending on the ligand concentration) a solid was formed, probably due to the low solubility of the neutral form of 4,6-bispyrenoyl Ins(1,2,3,5)P_4. The behaviour of 4,6-bispyrenoyl Ins(1,2,3,5)P_4 in the presence of Fe(III) was analysed also in 0.15 M Me_4NCl and at 37.0 °C. Nine potentiometric titrations were carried out (50–100 experimental points each titration), at ligand concentrations ranging from 0.2 to 0.4 mM and ligand to metal molar ratios from 0.7 to 2.2. Hydrolysis constants of Fe(III) under the same conditions were taken from previously reported data.[13] Potentiometric runs were carried out as previously described[12] with an automatic titrator Mettler Toledo T50. Either HCl or $Me_4N(OH)$ solutions were used as the titrant. The cell constants $E°$, and the liquid junction potentials were determined under the same conditions using the GLEE program.[40] The obtained data were analysed using the HYPERQUAD program.[41] In all cases, the fit of the values predicted by the model to the experimental data was estimated on the basis of the parameter σ corresponding to the scaled sum of square differences between predicted and experimental values. Then, the constants were used to produce species distribution diagrams using the HySS program.[42]

Hydroxyl radical assay

Ultra-violet (UV) absorbance were recorded on a ThermoSpectronic Unicam-300 spectrophotometer (UK) running Vision 32 software (version 1.25), using disposable 1.5 mL semi-micro cuvettes (path length 1 cm). The assay conditions employed were based on literature described by Hawkins and co-workers[9] and Graf and co-workers.[8,14] The standard assay mixture contained: 20 mM Trizma (Sigma) buffered to pH 7.5 with HCl, 50 mM dimethylsulfoxide, 0.3 mM hypoxanthine, 5 μM $FeCl_3$ (added

from a freshly prepared 50 μM stock solution) and 18 m-units of xanthine oxidase (Sigma; lyophilised powder from bovine milk). For the stock hypoxanthine solution, addition of 0.1 M NaOH solution prior to dilution with buffer was required to aid solubility. For each measurement, triplicate 1.0 mL samples were prepared containing the assay mixture and varying concentrations of chelator (added from 1 mM stock solution). The fractions were incubated at 37 °C for 30 min, and then quenched by immersion in a boiling-water bath for 2 min, followed by addition of 250 μL formaldehyde detection reagent. The formaldehyde detection reagent was prepared from 15 g of ammonium acetate, 0.3 mL of acetic acid and 0.2 mL of acetylacetone in a final volume of 100 mL of water. The fractions were incubated at 37 °C for 40 min to develop the colour attributed to the formation of diacetyldihydrolutidine, and the absorbance measured at 410 nm in diminished light. The blanks were incubated with heat-killed enzyme.

Acknowledgements

We thank the EPSRC for a studentship and PhD plus fellowship (DM) and the BBSRC for a CASE (Morvus Technologies) studentship (NR).

References

1 F. M. McConnell, S. B. Shears, P. J. L. Lane, M. S. Scheibel and E. A. Clark, *Biochem. J.*, 1992, **284**, 447–455.
2 P. J. French, C. M. Bunce, L. R. Stephens, J. M. Lord, F. M. McConnell, G. Brown, J. A. Creba and R. H. Michell, *Proc. R. Soc. London, Ser. B*, 1991, **245**, 193–201.
3 C. M. Bunce, P. J. French, P. Allen, J. C. Mountford, B. Moor, M. F. Greaves, R. H. Michell and G. Brown, *Biochem. J.*, 1993, **289**, 667–673.
4 C. J. Barker, J. Wright, C. J. Kirk and R. H. Michell, *Biochem. Soc. Trans.*, 1995, **23**, 169S.
5 C. J. Barker, P. J. French, A. J. Moore, T. Nilsson, P. -O. Berggren, C. M. Bunce, C. J. Kirk and R. H. Michell, *Biochem. J.*, 1995, **306**, 557–564.
6 I. D. Spiers, S. Freeman, D. R. Poyner and C. H. Schwalbe, *Tetrahedron Lett.*, 1995, **36**, 2125–2128.
7 I. D. Spiers, C. J. Barker, S. -K. Chung, Y. -T. Chang, S. Freeman, J. M. Gardiner, P. H. Hirst, P. A. Lambert, R. H. Michell, D. R. Poyner, C. H. Schwalbe, A. W. Smith and K. R. H. Solomons, *Carbohydr. Res.*, 1996, **282**, 81–99.
8 E. Graf, K. L. Empson and J. W. Eaton, *J. Biol. Chem.*, 1987, **262**, 11647–11650.
9 P. T. Hawkins, D. R. Poyner, T. R. Jackson, A. J. Letcher, D. A. Lander and R. F. Irvine, *Biochem. J.*, 1993, **294**, 929–934.
10 C. J. Barker, J. Wright, P. J. Hughes, C. J. Kirk and R. H. Michell, *Biochem. J.*, 2004, **380**, 465–473.
11 A. J. Letcher, M. J. Schell and R. F. Irvine, *Biochem. J.*, 2008, **416**, 263–270.
12 J. Torres, S. Dominguez, M. F. Cerda, G. Obal, A. Mederos, R. F. Irvine, A. Diaz and C. Kremer, *J. Inorg. Biochem.*, 2005, **99**, 828–840.
13 N. Veiga, J. Torres, D. Mansell, S. Freeman, S. Dominguez, C. J. Barker, A. Diaz and C. Kremer, *JBIC, J. Biol. Inorg. Chem.*, 2009, **14**, 51–59.
14 E. Graf, J. R. Mahoney, R. G. Bryant and J. W. Eaton, *J. Biol. Chem.*, 1984, **259**, 3620–3624.
15 I. D. Spiers, S. Freeman and C. H. Schwalbe, *J. Chem. Soc., Chem. Commun.*, 1995, 2219–2220.
16 D. Mansell, N. Rattray, L. L. Etchells, C. H. Schwalbe, A. J. Blake, E. V. Bichenkova, R. A. Bryce, C. J. Barker, A. Diaz, C. Kremer and S. Freeman, *Chem. Commun.*, 2008, 5161–5163.
17 L. G. Barrientos and P. P. N. Murthy, *Carbohydr. Res.*, 1996, **296**, 39–54.
18 B. Q. Phillippy and E. Graf, *Free Radical Biol. Med.*, 1997, **22**, 939–946.
19 S. D. Lytton, B. Mester, J. Libman, A. Shanzer and Z. I. Cabantchik, *Anal. Biochem.*, 1992, **205**, 326–333.
20 T. Palanche, F. Marmolle, M. A. Abdallah, A. Shanzer and A. -M. Albrecht-Gary, *JBIC, J. Biol. Inorg. Chem.*, 1999, **4**, 188–198.
21 M. M. Meijler, R. Arad-Yellin, Z. I. Cabantchik and A. Shanzer, *J. Am. Chem. Soc.*, 2002, **124**, 12666–12667.
22 Y. Ma, W. Luo, P. J. Quinn, Z. Liu and R. C. Hider, *J. Med. Chem.*, 2004, **47**, 6349–6362.
23 R. Kikkeri, H. Traboulsi, N. Humbert, E. Gumienna-Kontecka, R. Arad-Yellin, G. Melman, M. Elhabiri, A. -M. Albrecht-Gary and A. Shanzer, *Inorg. Chem.*, 2007, **46**, 2485–2497.
24 F. Fages, B. Bodenant and T. Weil, *J. Org. Chem.*, 1996, **61**, 3956–3961.
25 M. Kadirvel, E. V. Bichenkova, A. D'Emanuele and S. Freeman, *Chem. Lett.*, 2006, **35**, 868–869.
26 M. Kadirvel, B. Arsic, S. Freeman and E. V. Bichenkova, *Org. Biomol. Chem.*, 2008, **6**, 1966–1972.
27 C. Monahan, J. T. Bien and B. D. Smith, *Chem. Commun.*, 1998, 431–432.
28 H. -G. Weinig, R. Krauss, M. Seydack, J. Bendig and U. Koert, *Chem.–Eur. J.*, 2001, **7**, 2075–2088.
29 H. Yuasa, N. Miyagawa, T. Izumi, M. Nakatani, M. Izumi and H. Hashimoto, *Org. Lett.*, 2004, **6**, 1489–1492.
30 H. Yuasa, N. Miyagawa, M. Nakatani, M. Izumi and H. Hashimoto, *Org. Biomol. Chem.*, 2004, **2**, 3548–3556.
31 H. Dozol, C. Blum-Held, P. Guedat, C. Maechling, S. Lanners, G. Schlewer and B. Spiess, *J. Mol. Struct.*, 2002, **643**, 171–181.
32 T. -H. Kim and A. B. Holmes, *J. Korean Chem. Soc.*, 2006, **50**, 129–136.
33 C. A. Hunter and J. K. M. Sanders, *J. Am. Chem. Soc.*, 1990, **112**, 5525–5534.
34 B. A. Borgias, S. J. Barclay and K. N. Raymond, *J. Coord. Chem.*, 1986, **15**, 109–123.
35 B. Bodenant, F. Fages and M. -H. Delville, *J. Am. Chem. Soc.*, 1998, **120**, 7511–7519.
36 F. Fages, S. Leroy, T. Soujanya and J. -E. Sohna Sohna, *Pure Appl. Chem.*, 2001, **73**, 411–414.
37 C. J. Volkmann, G. M. Chateauneuf, J. Pradhan, A. T. Bauman, R. E. Brown and P. P. N. Murthy, *Tetrahedron Lett.*, 2002, **43**, 4853–4856.
38 X. Liu and F. J. Millero, *Mar. Chem.*, 2002, **77**, 43–54.
39 G. M. Sheldrick, *Acta Crystallogr., Sect. A: Found. Crystallogr.*, 2008, **64**, 112–122.
40 P. Gans and B. O'Sullivan, *Talanta*, 2000, **51**, 33–37.
41 P. Gans, A. Sabatini and A. Vacca, *Talanta*, 1996, **43**, 1739–1753.
42 L. Alderighi, P. Gans, A. Ienco, D. Peters, A. Sabatini and A. Vacca, *Coord. Chem. Rev.*, 1999, **184**, 311–318.

